Using the Differentiator-Smoother Filter to Analyze Traveling Waves on Transmission Lines: Fundamentals, Settings and Implementation

Felipe Lopes, Eduardo Leite Jr., João Paulo Ribeiro, Lilian Lopes, Artur Piardi, Rodrigo Otto, Washington Neves

***Abstract*—Modern solutions for transmission lines have increasingly used traveling wave (TW)-based functions, motivating the development of techniques to reliably identify fault-induced TWs that propagate along the monitored power grid. The Differentiator-Smoother filter (DS filter) has been successfully used in recent years in real-world TW-based applications, but the main concepts of this filter as used in real devices are somewhat new for utilities. Thus, this paper addresses the DS filter fundamentals, settings and implementation issues by means of electromagnetic transients simulations. The obtained results show that DS filter features are favorable for TW-based protection and fault location applications.**

***Keywords*—Differentiator-smoother filter, electromagnetic transients, power systems, traveling waves.**

I. Introduction

IN MODERN electrical power systems, transient-based algorithms have been increasingly used to improve transmission line monitoring solutions [1]. In this context, TW-based protection and fault location functions have attracted the interest of utilities, mainly because they are immune to sources of errors that usually affect traditional techniques based on the fundamental component analysis [2].

TWs are induced by events which lead the system to abruptly change its operation conditions, such as faults, switching maneuvers, lightning strokes, and so on [3]. As soon as these TWs reach the monitored points, distortions in current and voltage signals are generated, which are superimposed on the fundamental frequency signal. Thus, the TW analysis in transmission lines requires the use of appropriate filtering techniques with the capability of extracting accurate information regarding the arrival-time and amplitude of TWs at monitored terminals [4]. To do so, digital high- and band-pass filters are usually applied to separate the fundamental component from the transient signals [5], [6].

Felipe Lopes, Eduardo Leite Jr. and João Paulo Ribeiro are with the Department of Electrical Engineering at University of Brasília (UnB), 70910-900 Brasília-DF, Brazil. (e-mail: felipevlopes@ene.unb.br, eduardoleitejr@gmail.com, joaopaulogribeiro@gmail.com).

Lilian Lopes is with the WFA Consulting, 58037-030 João Pessoa-PB, Brazil. (e-mail: liliangda@gmail.com).

Artur Piardi and Rodrigo Otto are with the Laboratory of Electrical Power Systems (LASSE), Itaipu, Foz do Iguaçu-PR, (e-mail: artur.piardi@pti.org.br, rodrigobueno@pti.org.br).

Washington Neves is with the Department of Electrical Engineering of Federal University of Campina Grande (UFCG) (e-mail: waneves@dee.ufcg.edu.br).

Paper submitted to the International Conference on Power Systems Transients (IPST2019) in Perpignan, France, June 17-20, 2019.

Several transient detection methods have been proposed over the recent decades to aid TW-based fault location and protection schemes, such as: Discrete Wavelet Transform (DWT) and Maximal Overlapped Discrete Wavelet Transform (MODWT) [7], [8], Park's transformation (TDQ) [9]; Finite Impulse Response (FIR) filters [6]; Differentiator-Smoother filter [1], [2], called here DS filter; among others.

Both DWT and MODWT have been widely applied in TW-based solutions. They apply a cascade of high-pass and low-pass filters, whose coefficients are set based on the chosen mother wavelet [10]. Unlike the MODWT, the DWT requires a downsampling procedure, which reduces the signal resolution in time. Hence, the MODWT have been the most used in TW-based applications, although its performance is still dependent on the chosen mother wavelet [11].

The TDQ application for TW detection purposes in a fault location scheme was firstly reported in [9]. It has the advantage of being sensitive to transients and phase imbalances as well, being able to detect the sought TWs even in cases of attenuated transients. Nevertheless, it is not able to separately analyze transients in each system phase [9], which is a procedure required by many TW-based line protection functions.

The FIR digital filters have been applied in real-world TW-based fault location schemes for years [6]. However, it is known that spurious transients may show up in the filter outputs and TW content may be lost in some cases, depending on the chosen cut-off frequencies at which the filters are set to operate. As a result, similarly to the DWT and MODWT, preliminary studies are usually required to properly select the settings to be considered.

Aiming to overcome the difficulties faced by most TW detection algorithms, in [1] and [2], the DS filter is proposed for TW-based fault location and protection applications, respectively. This filter creates patterns on its outputs which can be related to the arrival time of TWs at the monitored points, maintaining an unitary gain [2]. However, although the DS filter has been already used in actual time-domain relays, details on its fundamentals, settings and implementation are still scarce in the literature. Thus, this paper shows how the DS filter operates, highlighting the settings that must be applied to obtain an unitary gain in practical applications, as well as studies on relevant implementation and operation issues. Also, frequency response, coefficients window length effects and potential applications are also pointed out, providing support for researchers and utilities interested in evaluating TW on transmission lines by using the DS filter.

II. Fault-Induced TWs on Transmission Lines

The DS filter was developed to produce patterns in its outputs with the aim to facilitate the analysis of fault-induced TWs. Therefore, to understand the DS filter operation, typical transients induced by faults must be firstly studied.

When a fault occurs on a transmission line, the fault point voltage v_f collapses, making the transmission line to abruptly change its operation condition. In a solid fault case, for instance, v_f suddenly varies from the pre-fault voltage value to zero volts, thereby a step change with amplitude equal to the negative of the voltage variation is verified in voltage signals in the faulted phase. These transients propagate as TWs along the line, until they reach the line ends where the TW detectors are installed [1]. Such a phenomena can be explained through the pure fault circuit shown in Fig. 1, from which the TWs launched on the line can be analyzed, being R_f the fault resistance, Z_c the line characteristic impedance, v_f the pre-fault voltage at the fault point and $v_{f,TW}$ the amplitude of the TWs launched on the line for a three-phase short-circuit.

In Fig. 1, the line terminations are not depicted because they do not affect the amplitude of the TWs launched on the line, but only the measured TWs at the line ends [1]. Thus, being $v_f \approx V_{rated} \cdot \sin(\theta)$ at the fault inception time, where V_{rated} is the line rated phase-to-neutral voltage and θ is the fault inception angle, $v_{f,TW}$ can be calculated by means of a voltage divider formed by R_f and the parallel of the line sections upstream and downstream the fault point:

$$v_{f,TW} = \frac{Z_c \cdot V_{rated} \cdot \sin(\theta)}{Z_c + 2 \cdot R_f} \ , \tag{1}$$

being the current TW $i_{f,TW}$ amplitude given by:

$$i_{f,TW} = \frac{v_{f,TW}}{Z_c} = \frac{V_{rated} \cdot \sin(\theta)}{Z_c + 2 \cdot R_f} \ . \tag{2}$$

From (1) and (2), the following conclusions are taken: 1) When a TW reach the line terminal, step changes in voltages and currents are verified. Few moments after, the induced wavefronts overlap, generating transients with different formats; 2) For high values of R_f and when $\theta \approx 0°$ or $\theta \approx 180°$ (voltage zero-crossings for a sinusoidal reference), no voltage step change at the fault point is verified, thereby TWs are not launched. Thus, the importance of having filters with unitary gain whose outputs create patterns related to step changes is demonstrated. Indeed, such a behavior facilitates the evaluation of TWs amplitudes and polarities, making it easier to set thresholds in TW detectors, as well as avoiding confusion between spurious transients and TWs.

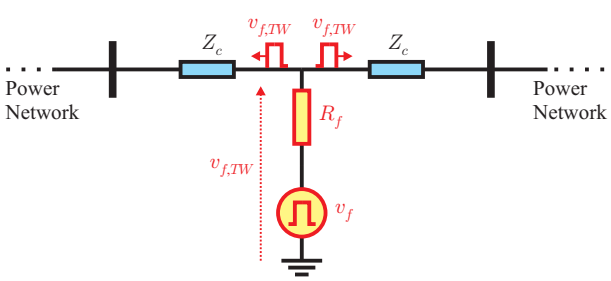

Fig. 1. Fault-induced TWs launched on the line.

III. The DS Filter

Fig. 2 presents the DS filter coefficients window and the output format for step changes in the input signal [2]. It is noteworthy to emphasize that the DS filter developers opted for the generation of a triangular-shaped output with unitary gain in cases of step changes in the input signal rather detecting high frequency signals only, as traditional methods usually do, facilitating the TW detection procedure [1]. Hence, the moment at which the triangle-shaped output peak occurs is associated to the arrival time of TWs at the monitored terminal. Moreover, such a triangular format facilitates the parabola-based sample interpolation process, which will be addressed in the next sections [1].

A. Setting DS Filter to Obtain an Unitary Gain

In Fig. 2(b), it is observed that the DS filter triangular output amplitude is equal to the one of the input step change. Such an unitary gain is only possible when an appropriate gain setting G of the N_{DS} DS filter coefficients is chosen. As shown in Fig. 2(a), half of the DS filter coefficients has the value G, being the other half set to $-G$ value (this paper disregards null central coefficients). Thus, the G value must be obtained for any number of coefficients N_{DS}, which is a procedure not properly described in the open literature.

In order to guarantee that the setting G will yield an unitary gain in the DS filter outputs, consider the example shown in Fig. 3, where the DS filter coefficients window slides over a current signal in the form of step with amplitude A. In the figure, three stages are highlighted: Stage 1) The DS filter coefficients window is completely within the region before the step change; Stage 2) Moment at which the coefficients window is centered on the rising edge of the step; and Stage 3) The DS filter coefficients window is completely within the region after the step change, with amplitude A. Thus, as the DS filter output is given by the inner product between the input signal samples and the filter coefficients (as shown in Fig. 3), the output values i_{TW} for each stage are obtained:

$$\begin{aligned} \textbf{Stage 1: } i_{TW} &= 0.5 \cdot N_{DS}(-G \cdot 0) + 0.5 \cdot N_{DS}(G \cdot 0) \\ &= 0. \end{aligned} \tag{3}$$

$$\begin{aligned} \textbf{Stage 2: } i_{TW} &= 0.5 \cdot N_{DS}(-G \cdot 0) + 0.5 \cdot N_{DS}(G \cdot A) \\ &= 0.5 \cdot N_{DS} \cdot G \cdot A. \end{aligned} \tag{4}$$

$$\begin{aligned} \textbf{Stage 3: } i_{TW} &= 0.5 \cdot N_{DS}(-G \cdot A) + 0.5 \cdot N_{DS}(G \cdot A) \\ &= 0. \end{aligned} \tag{5}$$

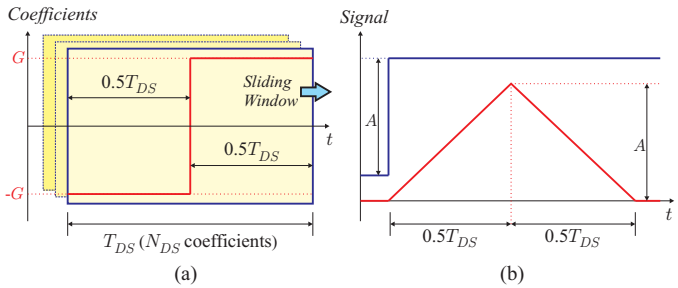

Fig. 2. DS filter: (a) Coefficients window; (b) Filter response to step changes.

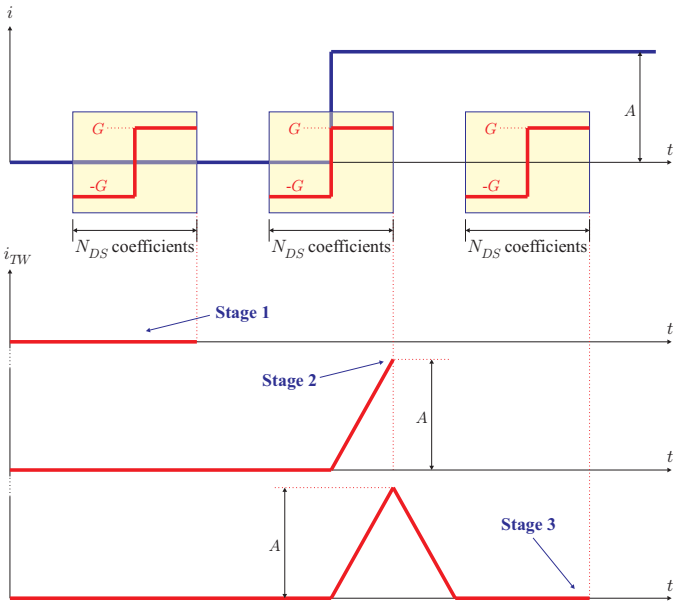

Fig. 3. Calculating the setting G to obtain an unity gain.

It is observed that i_{TW} is zero when the DS filter coefficients window is completely inside the regions before and after the step change where the input signal is constant (Stages 1 and 3). On the other hand, the DS filter output assumes its maximum value in Stage 2, when the coefficients window is aligned with the rising edge of the step change in the input signal. Therefore, as $i_{TW} = A$ must be obtained in Stage 2, it can be proven that $G = \frac{2}{N_{DS}}$ must be set.

Fig. 4 shows the DS filter outputs considering a fault current signal simulated in the Alternative Transients Program (ATP). The amplitudes A_1, A_2 and A_3 of the fault-induced TWs and the associated DS filter outputs are highlighted considering $G = \frac{2}{N_{DS}}$. As expected, triangle-shaped signal variations with amplitude similar to those of the step changes are observed, preserving the polarity information of each TW.

B. DS Filter Coefficients Window Length

The DS filter coefficients window length can be represented as the time period T_{DS}, which is the result of N_{DS} coefficients for a given sampling period Δt, as shown in Fig. 2. Thus, one can calculate $N_{DS} = \lfloor \frac{T_{DS}}{\Delta t} \rfloor$, where $\lfloor \cdot \rfloor$ stands for the function *floor*, which gives as output the greatest integer less than or equal to the argument.

It can be demonstrated that different output signals are obtained by changing T_{DS}. As depicted in Fig. 2, the width of the triangular output is equal to the coefficients window length, so that, depending on the adopted T_{DS} value, filtered signal variations can overlap, affecting the interpretation of measured fault-induced TWs. To illustrate such an issue, Fig. 5 presents the DS filter application considering $T_{DS} = 20$ μs, 160 μs and 320 μs, being $\Delta t = 1$ μs. It is noticed that the greater T_{DS} is, the longer the DS filter coefficients window takes to align with the rising edge of the input signal step change. Thus, the width of the triangular output increases, jeopardizing the detection of TWs that reach the monitored point at instants close to each other. For instance, in the case shown in Fig. 5, using $T_{DS} = 20$ μs and 160 μs, the two first consecutive TWs can be detected, but using $T_{DS} = 320$ μs, the detection of the second wavefront is compromised, since the two first triangular outputs overlap, so that only one wavefront seems to have arrived at the monitored terminal.

C. DS Filter Frequency Response

Analyzing Fig. 5, it is observed that different T_{DS} values result in different DS filter outputs. In the first few instants depicted Fig. 5, it is observed that the DS filter outputs present quasi-constant values, which differ from one to another. In fact, depending on the chosen T_{DS} value, different DS filter frequency responses are verified, as illustrated in Fig. 6 for $T_{DS} = 20$ μs, 160 μs and 320 μs, where the filter gain in the region around power frequency (here taken as 60 Hz) is highlighted. To obtain Fig. 6, a sampling period $\Delta t = 1$ μs was used, which results in a sampling frequency $f_s = 1$ MHz. Therefore, frequency responses are illustrated up to 500 kHz, respecting the Nyquist criterion.

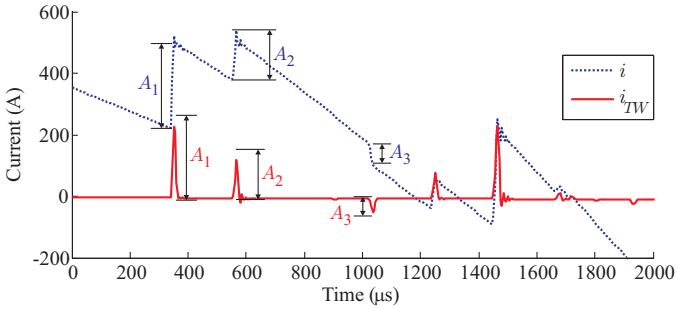

Fig. 4. Example of DS filter application in a simulated current fault record.

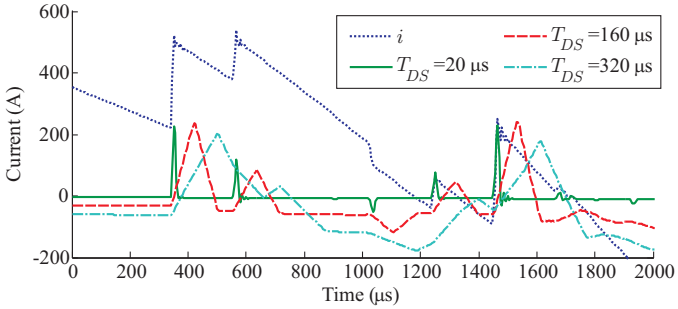

Fig. 5. T_{DS} influence on the DS filter performance.

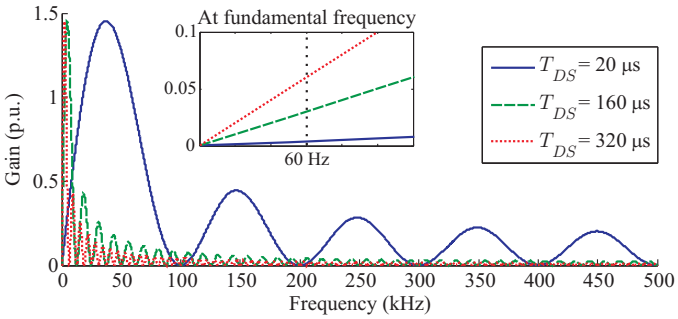

Fig. 6. DS filter frequency response considering different T_{DS} values.

As shown in Fig. 6, when T_{DS} increases, the attenuation of high frequency components also increases. For instance, considering $T_{DS} = 20$ μs, frequencies close to 100 kHz, 200 kHz, 300 kHz, 400 kHz and 500 kHz are greatly attenuated, whereas those in between 100-200 kHz, 200-300 kHz, 300-400 kHz and 400-500 kHz have enough gain to sensitize the DS filter outputs. On the other hand, by increasing T_{DS}, frequencies from 100 kHz onwards are more attenuated, which corroborates with the analysis presented earlier, in which the use of high T_{DS} values is not adequate to evaluate rapid changes in the input signals. It should be also observed that the smaller the T_{DS} value, the more attenuated the power frequency (here, 60 Hz) will be, explaining the different offset values verified in the first instants of Fig. 5, which are actually the fundamental component seen in a microsecond scale.

The presented findings are of utmost importance for TW detection procedures. Indeed, if the triangular DS filter output is superimposed by some fundamental component content and the DS filter output peak is inside a valley of the fundamental frequency signal, it is not possible to define a hard threshold to detect such a wavefront [12], because the fundamental component maximum values will exceed the DS filter output peak value. Thus, TW detection problems may arise, thereby the use of small T_{DS} values is indicated. Indeed, $T_{DS} = 20$ μs is used in actual TW-based relays which use the DS filter [13].

The presented frequency response results may seem strange regarding the limited DS filter output bandwidth, since TW-based methods usually depend on the analysis of high-frequency signals. However, one should bear in mind that the DS filter was designed to respond with unitary gain to step-changes only, which are indeed the transients related to fault-induced TWs that reach the monitored line terminals.

D. Analyzing Attenuated TWs

It is well-known that fault-induced TWs attenuate during their propagation along the line. Also, depending on the point on the wave the fault takes place, overdamped transients may be verified. Hence, the step changes expected to be measured at the monitored line ends may appear as ramp changes in monitored signals, whose rate of variation from the initial value to the final one depends on the fault-induced TWs attenuation level. Thus, to evaluate the DS filter performance when ramp changes occur in monitored signals rather than step changes, Fig. 7 presents the DS filter time response considering four input signals with different dispersion levels caused by fault-induced transient attenuation.

The Input 1 shown in Fig. 7 presents a very high variation rate, i.e., it can be taken as a step change. Thus, as expected, a triangle-shaped output with unitary gain is verified, with peak value occurring at about $\frac{T_{DS}}{2}$ seconds after the step change. On the other hand, Inputs 2, 3 and 4 are ramp changes with rates of variation smaller than the one observed in Input 1. In these cases, parabola-shaped outputs are observed, whose peak values do not match exactly the ramp signal amplitude. Indeed, the smaller the ramp signal rate of variation, the greater is the dispersion of the DS filter outputs, what can obviously jeopardize the TW detection process, resulting in additional errors in the estimated TW arrival times and amplitudes.

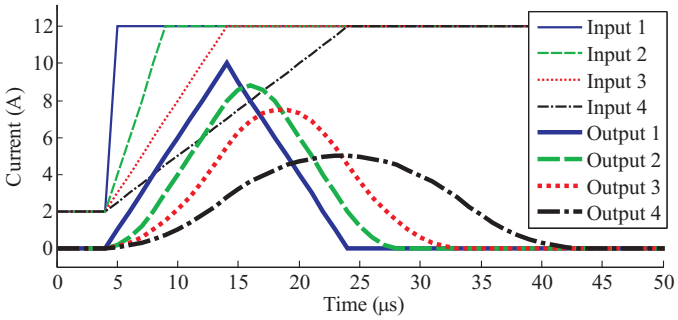

Fig. 7. DS filter outputs in cases of attenuated transients.

IV. Practical Processing of DS Filter Outputs to Estimate TW Amplitude and Arrival Time

As explained in the previous sections, the DS filter outputs may present dispersion due to transients attenuation and signal time resolution, causing errors in the TW amplitude and arrival time estimations. Even so, the signal patterns created in DS filter outputs can be processed in order to reduce errors in estimated amplitude and arrival time, improving TW-based protection and fault location applications. Details on these signal processing procedures are not properly addressed in the literature, thereby this section presents studies on these issues.

A. TW Amplitude Estimation

When the DS filter is applied, it seems that the peak detection is enough to guarantee a reliable TW amplitude estimation. However, it is true only in cases of inputs in the form of step changes, thereby the DS filter output peak value may not represent the correct TW amplitude in cases of attenuated transients. Hence, additional procedures are usually taken into account to obtain a more accurate estimation.

In [2], two-terminal measurements of TW amplitude are taken to implement a TW-based differential protection scheme. It is shown that the amplitude I of a given wavefront can be estimated from the DS filter output i_{TW} by using:

$$I = C \cdot \sum_{n=-M}^{n=M} i_{TW}(N_{detec} - n) \ , \tag{6}$$

where N_{detec} is the sample at which the wavefront was detected, M is the number of samples around the peak value to be taken into account in the calculations, being suggested $M = 0.5N_{DS}$, and C is a setting called scaling factor, which is used to maintain the unitary gain of I.

Although the use of (6) is computationally simple, from the authors' best knowledge, the calculation of the setting C to obtain unitary gain is not presented in the open literature. Thus, to investigate such a question, Fig. 8 presents the DS filter response to a step change, highlighting M samples around the peak value and the lines formed by each side of the triangle-shaped output, which are mathematically derived as:

$$f_1(n) = (2A/N_{DS}) \cdot n \ , \tag{7}$$

$$f_2(n) = -(2A/N_{DS}) \cdot n + 2A \ , \tag{8}$$

where n and $f(n)$ represent the horizontal and vertical Cartesian axes in Fig. 8(b), respectively.

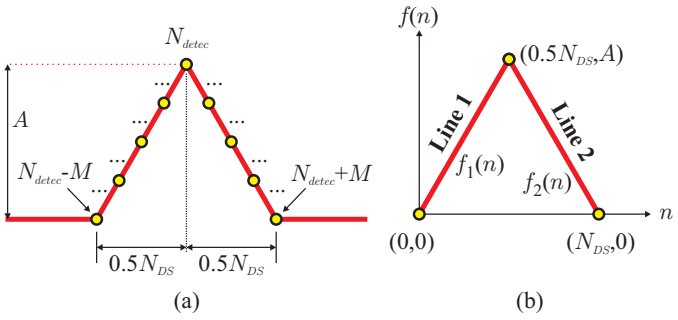

Fig. 8. TW amplitude estimation: (a) Samples around the DS filter output peak value; (b) Analyzing DS filter output lines to obtain the TW amplitude.

According to (6), the sum of the M samples before and after the triangle-shaped output peak value must be equal to the TW amplitude A. Thus, as $f_1(n)$ and $f_2(n)$ are valid for the first and second half of the DS filter output samples, respectively, and considering that the peak value is a common point, by using $M = 0.5N_{DS}$, the following equation can be obtained for $n = 0,\ 1,\ 2,...,\ N_{DS}$:

$$A = C \cdot \left(\underbrace{\sum_{n=0}^{n=\frac{N_{DS}}{2}} f_1(n)}_{\sum f_1} + \underbrace{\sum_{n=\frac{N_{DS}}{2}+1}^{N_{DS}} f_2(n)}_{\sum f_2} \right) , \qquad (9)$$

being:

$$\sum f_1 = \frac{2A}{N_{DS}} \left(0 + 1 + 2 + ... + \frac{N_{DS}}{2} \right) , \qquad (10)$$

$$\sum f_2 = \frac{N_{DS}A}{2} - \frac{2A}{N_{DS}} \left(0 + 1 + 2 + ... + \frac{N_{DS}}{2} \right) . \qquad (11)$$

As a result, from (9), it is concluded that $C = \frac{2}{N_{DS}}$ must be set to guarantee the unitary gain in the TW amplitude measurement in cases of triangle-shaped DS filter outputs. It should be pointed out that as the DS filter output becomes a parabola-shaped signal, the errors in the estimated TW amplitude increase. However, by using (6) with the appropriate scaling factor C, these errors are reduced in comparison to the deviations observed when only the peak value is taken into account. To demonstrate such an issue, Table I shows the obtained results for the current signals illustrated in Fig. 7, in which a TW amplitude equal to 10 A must be estimated.

From the results, as expected, it is verified that for cases in which a step-change occurs in the DS filter input signal, the estimated TW amplitude error is negligible. However, as the transients attenuate, making the step-changes to appear at the monitored terminals as ramp-changes, the errors increase. Even so, even in the worst analyzed case (Output 4 in Fig. 7), the TW amplitude estimation error did not exceed 15% in relation to the actual value, attesting that the application of (6) in the DS filter outputs is useful for TW-based approaches which require the analysis of TW amplitudes.

TABLE I
REDUCING ERRORS IN THE TW AMPLITUDE ESTIMATION.

Output Signal	Peak Value	Estimated Amplitude Using (6)	|Percentage Error| Peak	|Percentage Error| Via (6)
Output 1*	10.00 A	10.00 A	0.00%	0.00%
Output 2	8.80 A	9.96 A	12.00%	0.40%
Output 3	7.50 A	9.70 A	25.00%	3.00%
Output 4	5.00 A	8.58 A	50.00%	14.25%

*Case of step-change in the DS filter input signal.

B. TW Arrival Time Detection

Although the TW amplitude directly interfere in the fault-induced transient detection process, in most TW-based techniques, specially in fault location ones, the TW arrival time at monitored points is the crucial information to be extracted from the filtered signals [5]. As a consequence, fault records time resolution is often reported as one of the most important issues for TW-based techniques, which require the use of sampling frequencies in the order of MHz [1]. Therefore, the greater the sampling frequency f_s, the smaller the sampling period Δt, making the signal time resolution better, and allowing a more accurate TW arrival time detection at the monitored points.

The triangular and parabolic patterns created in the DS filter outputs is taken as an advantageous feature. It permits an excellent data interpolation of the DS filter output, approximating it by a parabola with additional samples, which are used to reduce the errors in the TW arrival time detection that would be verified when the original signals are analyzed. Fig. 9 shows an example of the parabola-based interpolation reported in [1], through which the number of samples in DS filter output signal is increased by five times. In this case, $T_{DS} = 20\ \mu$s and $\Delta t = 1\ \mu$s and, to make the analysis more realistic, an attenuated transient signal was taken as the DS filter input, resulting in a parabola-shaped output with width little larger than T_{DS}. From Fig. 9, it is noticed that different peak detections occur before and after the interpolation process. Although the time difference between the peaks obtained from the original and interpolated signals is not relevant, in a real-world fault location procedure, the interpolation process may reduce the absolute fault distance errors from several hundreds of meters to few dozens of meters, achieving an accuracy of about a typical tower span [1]. To exemplify the interpolation process, solid AG faults initiated at the fault point voltage peak in the 230 kV/60 Hz line depicted in Fig. 10 were analyzed. Table II shows the fault location results obtained from the classical two-terminal TW-based fault location method with and without interpolation process, being the estimated fault distance $\widetilde{d}$ obtained by:

$$\widetilde{d} = 0.5\left[\ell - (t_R - t_L) \cdot v\right] , \qquad (12)$$

where ℓ is the line length, t_L and t_R are the first incident TW arrival times at the local and remote line ends, respectively, and v is the aerial mode TW propagation velocity.

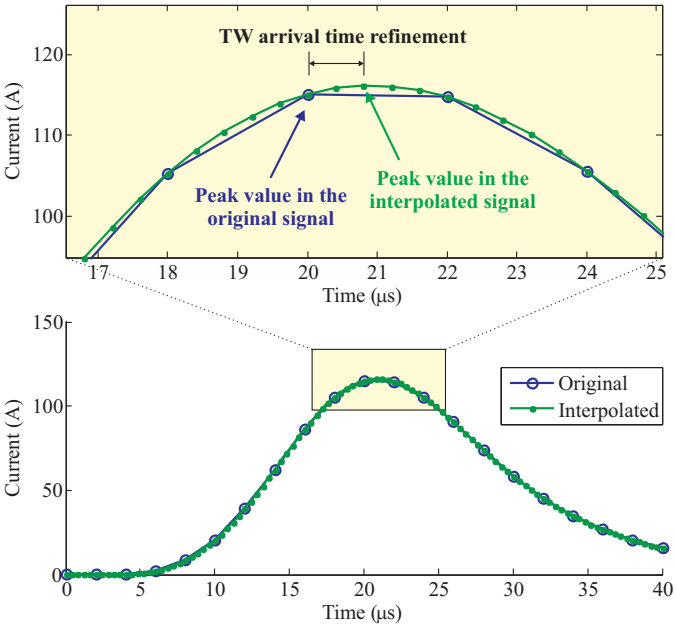

Fig. 9. Example of the DS filter output parabola-based interpolation process.

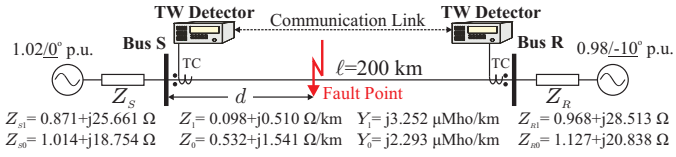

Fig. 10. Test 230 kV/60 Hz power system.

TABLE II
DS FILTER OUTPUT INTERPOLATION IN FAULT LOCATION PROCEDURES.

Actual Fault Distance d	**Estimation** $\widetilde{d}$ **Without Interpolation**	**Estimation** $\widetilde{d}$ **With Interpolation**
20 km	19.88 km	19.99 km
60 km	60.09 km	59.99 km
100 km	100.00 km	100.00 km
140 km	139.91 km	140.00 km
180 km	180.12 km	180.00 km

Table II shows that the benefits of the interpolation process are less evident when faults take place close the middle of the line. In these cases, the TWs dispersion tends to be similar at both line ends, thereby associated errors are canceled in (12). However, in cases of faults close to the line ends, the TW dispersion levels at the monitored points are different, so that the DS filter output interpolation process shows to be more beneficial, reducing the fault location errors from hundreds of meters to few meters. In practice, although the use of the original DS filter outputs is promising, the fault location error reduction achieved through the parabola-based interpolation is still advantageous, since it can avoid unnecessary inspection of adjacent lines in cases of close-in/far-end faults, in which the fault location errors are more significant.

V. CONCLUSIONS

In this work, the Differentiator-Smoother filter (DS filter) was studied. Firstly, typical fault-induced transients were addressed to facilitate the understanding of the DS filter concepts, and then, details on the filter settings and implementation issues were pointed out.

It was shown that there is an specific setting of the DS filter coefficients that guarantee the filter unitary gain. Also, it was proven that the DS filter settings depend on the filter coefficients window length, which in turn also interfere in the DS filter frequency response. Then, in a second part of the paper, the procedures to estimate TW amplitude and arrival time from the DS filter outputs were described, highlighting practical cases in which the errors may be more expressive.

Although the DS filter requires high sampling rates to provide accurate fault-induced wavefront arrival detection as other existing TW detection methods do, the obtained results show it is promising for TW-based approaches, mainly when the analysis of TW amplitude is required. In fact, the DS filter is easy to implement and set, yielding very clean outputs, through which transients related to TWs can be easily detected.

ACKNOWLEDGMENT

The authors would like to thank the Brazilian National Council for Scientific and Technological Development (CNPq), the Coordination for the Improvement of Higher Education Personnel (CAPES) and the Itaipu Technological Park Foundation (FPTI) for the financial and technical support.

REFERENCES

[1] E. O. Schweitzer, A. Guzmán, M. V. Mynam, V. Skendzic, B. Kasztenny, and S. Marx, "Locating faults by the traveling waves they launch," in *50th Annual Minnesota Power Systems Conference*, November 2014.

[2] E. Schweitzer, B. Kasztenny, and M. V. Mynam, "Performance of time-domain line protection elements on real-world faults," in *42nd Annual Western Protective Relay Conf.*, Oct. 2015.

[3] A. Greenwood, *Electrical Transients in Power Systems*. New York, USA: 2nd Edition, John Wiley and Sons, 1991.

[4] F. B. Costa, B. A. Souza, and N. S. D. Brito, "Real-time detection of fault-induced transients in transmission lines," *IET Electronics Letters*, pp. 753–755, May 2010.

[5] M. M. Saha, J. Izykowski, and E. Rosolowski, *Fault Location on Power Networks*, ser. Power Systems. London: Ed. Springer, 2010.

[6] S. L. Zimath, M. A. F. Ramos, and J. E. S. Filho, "Comparison of impedance and travelling wave fault location using real faults," in *2010 IEEE/PES Trans. and Dist. Conf. and Exposition*, April 2010, pp. 1 –5.

[7] F. B. Costa, B. A. Souza, and N. S. D. Brito, "A wavelet-based algorithm to analyze oscillographic data with single and multiple disturbances," in *2008 IEEE/PES General Meeting*, July 2008, pp. 1–8.

[8] F. B. Costa, "Boundary wavelet coefficients for real-time detection of transients induced by faults and power-quality disturbances," *IEEE Transactions on Power Del.*, vol. 29, no. 6, pp. 2674–2687, Dec 2014.

[9] F. V. Lopes, D. Fernandes, and W. Neves, "A traveling-wave detection method based on Park's transformation for fault locators," *IEEE Transactions on Power Delivery*, vol. 28, no. 3, pp. 1626–1634, 2013.

[10] D. B. Percival and A. T. Walden, *Wavelet Methods for Time Series Analysis*. New York, USA: Cambridge University Press, 2000.

[11] F. Costa, A. Sobrinho, M. Ansaldi, and M. Almeida, "The effects of the mother wavelet for transmission line fault detection and classification," in *3rd International Youth Conf. on Energetics*, July 2011, pp. 1 –6.

[12] S. Santoso, E. Powers, W. Grady, and P. Hofmann, "Power quality assessment via wavelet transform analysis," *IEEE Transactions on Power Delivery*, vol. 11, no. 2, pp. 924 –930, apr 1996.

[13] *Ultra-High-Speed Transmission Line Relay Traveling-Wave Fault Locator High-Resolution Event Recorder*, SEL Schweitzer Engineering Laboratories, 2017.